Crystallization Processes

International Edition: DOI: 10.1002/anie.201500304
German Edition: DOI: 10.1002/ange.201500304

Shape without Structure: An Intriguing Formation Mechanism in the Solvothermal Synthesis of the Phase-Change Material Sb_2Te_3**

*Tobias Saltzmann, Manuel Bornhöfft, Joachim Mayer, and Ulrich Simon**

Abstract: *We introduce a novel solvothermal synthesis of individual single crystalline Sb_2Te_3 micro- and nanocrystals as a model material for phase-change switching. We identified different intermediates along the reaction path to the final Sb_2Te_3 hexagonal platelets (HPs) and discuss their forming mechanism. By means of nanodiffraction (ND) in a scanning transmission electron microscope we demonstrate that the intermediates follow a hexagonal shape evolution in the amorphous state. In situ nanomanipulator measurements reveal electrical phase-change switching properties of the individual Sb_2Te_3 hexagonal platelets.*

Sb_2Te_3 is receiving increasing attention in materials chemistry and technology.[1] It holds promise for applications, for example, as a thermoelectric material for converting thermal into electric energy,[2] as a topological insulator, representing a new state of quantum matter,[3] or as a phase-change material, which exhibits physical properties, such as reflectivity and resistivity, that change by orders of magnitude when the structure is altered from amorphous to crystalline and vice versa. These reversible phase-change properties are of particular interest in nonvolatile data storage devices.[4] Sb_2Te_3 crystallizes in the tetradymite structure and belongs to the space group $R\bar{3}m$ (lattice constants $a = 4.264$ and $c = 30.458$ Å).[5] Its structure is composed of hexagonal close-packed planes of Sb and Te running perpendicular to the trigonal axes. Five planes in the order of Te_1-Sb-Te_2-Sb-Te_1 form quintuple layers (QL) with a thickness of about 1 nm which are covalently bound. Between these Te-terminated quintuple layers, weak van der Waals forces dominate, but a covalent binding portion in the inter-quintuple-layer binding has to be taken into account as well.[6] Sb_2Te_3 is considered as a model compound for phase-change materials as it lies at one end of the pseudo binary tie line to GeTe where the most used ternary alloys of phase-change materials can be found.[7]

For application as a resistively switching phase-change material, Sb_2Te_3 has to exist in at least two characteristically different nonvolatile states, an amorphous and a crystalline one. These can be transferred into one another by the application of an external stimulus, such as an electric pulse. While Sb_2Te_3 exhibits almost metallic conductivity in the crystalline state (low resistance state; LRS), the amorphous state is characterized by an orders of magnitude higher resistivity (high resistance state; HRS).

In detail the transition from LRS to HRS is achieved by a short intense electric pulse and is described as a RESET process. Thereby the crystalline phase is locally melted and subsequently solidified forming an amorphous region owing to the fast quenching of the surrounding matrix. The LRS is achieved by a SET process, that is, crystallizing an amorphous region through a moderate electric pulse. The heat generated by this pulse owing to ohmic loss must be large enough to reach the glass temperature of the amorphous material and thus to enable (re)crystallization.[8]

For most applications Sb_2Te_3 is produced by gas-phase deposition methods, such as sputter-, MOCVD- or epitaxial deposition techniques, which have their own intrinsic advantages and disadvantages.[9] While sputter deposition is an inexpensive, industrially established deposition method, it leads to the formation of polycrystalline films. MOVCD and epitaxial deposition allow highly ordered single-crystalline structures to be fabricated. However, these methods require expensive and partially toxic starting materials as well as elaborated high vacuum technology. To understand structure–property relations in phase-change materials in general and to further improve device properties, it would be highly desirable to fabricate Sb_2Te_3 as single crystals with a low concentration of defects and defined morphology.

It has been demonstrated that Sb_2Te_3 single crystals can be obtained by solution-based syntheses. For example, Zhao et al. and Kim et al. reported the synthesis of plate-like particles by letting an antimony source react with trioctylphosphinetelluride in phenyl ether or oleic acid, respectively.[10] Partially intergrown platelets were synthesized by the decomposition of organometallic single-source precursors in high boiling solvents.[11] However, these routes require either the handling of highly toxic compounds or the sophisticated preparation of specific precursor compounds.

Solvothermal or hydrothermal approaches apply antimony and tellurium oxides or elemental tellurium, respec-

[*] T. Saltzmann, Prof. Dr. U. Simon
Institut für Anorganische Chemie
RWTH Aachen University
Landoltweg 1, 52074 Aachen (Germany)
E-mail: U.Simon@ac.rwth-aachen.de
M. Bornhöfft, Prof. Dr. J. Mayer
Gemeinschaftslabor für Elektronenmikroskopie
RWTH Aachen University
Ahornstrasse 55, 52074 Aachen (Germany)
T. Saltzmann, M. Bornhöfft, Prof. Dr. J. Mayer, Prof. Dr. U. Simon
JARA—Fundamentals of Future Information Technologies
RWTH Aachen University
Ahornstrasse 55, 52074 Aachen (Germany)

[**] We are grateful to the German Research Foundation (DFG) for funding this work through the SFB 917 ("Nanoswitches"). We thank Dr. Melanie Homberger for helpful discussions and Felix Schrader for the TEM and SEAD measurements on Intermediate 1 shown in Figure S2 d and e in the Supporting Information.

Supporting information for this article is available on the WWW under http://dx.doi.org/10.1002/anie.201500304.

tively, as less demanding and air stable starting materials, yielding Sb_2Te_3 nano- and microcrystals. The formation of Sb_2Te_3 is thereby performed in a closed reaction vessel in basic media in the presence of glycols, polymeric capping agents, water and, depending on the applied OH^- concentration, a reducing agent.[12]

In general the resulting products are composed of crystalline Sb_2Te_3 hexagonal platelets (HPs), where the shape is dictated by the trigonal elementary cell. Hence, the forming mechanism of Sb_2Te_3 hexagonal platelets is assigned to intrinsically anisotropic growth.[13] The hexagonal platelets typically have lateral sizes between several hundred nanometers and tens of micrometers and a thickness of up to five hundred nanometers. However, the crystals formed are often twinned and intergrown and it is still a great challenge to synthesize single crystals with a low defect concentration. Therefore, a detailed study of the formation mechanism would be of fundamental interest.

Herein we report an intriguing formation mechanism in the solvothermal synthesis of single-crystalline Sb_2Te_3 hexagonal platelets. We identified different intermediates along the reaction path towards the final crystalline Sb_2Te_3 hexagonal platelets. Of these intermediates some exhibit a hexagonal and layered shape as observed in AFM and electron microscopy measurements, suggesting a crystalline state, whereas electron nanodiffraction measurements indicate an amorphous state. Hence, the hexagonal shape of these intermediates is formed before a crystalline structure appears. Furthermore we show for the first time resistive switching properties of individual crystalline Sb_2Te_3 hexagonal platelets by means of in situ nanomanipulator measurements.

The preparation of Sb_2Te_3 hexagonal platelets was performed in a Teflon-lined autoclave by heating antimonyoxide and telluriumdioxide in the presence of polyvinylpyrrolidone (PVP) in diethylene glycol and sodium diethylene glycolate under solvothermal conditions at 200 °C. To analyze the hexagonal platelet formation mechanism, the reaction was quenched to room temperature at different points in time and the respective intermediates were separated by centrifugation and examined by means of scanning electron microscopy (SEM), energy-dispersive X-ray spectroscopy (EDX), powder X-ray diffraction (XRD), bright-field transmission electron microscopy (TEM), selected-area electron diffraction (SAED), and nanodiffraction (ND) performed in a scanning transmission electron microscope (STEM).

The reaction starts with the dissolution and reduction of the starting materials in accord with observations made by Zhang et al.[14] Under reaction conditions, in which, sodium diethylene glycolate is used as a base, intermediates with four distinguishable morphologies that form during the solvothermal synthesis of Sb_2Te_3 hexagonal platelets have been identified. These intermediates will be further denoted as Intermediate 1, 2, 3, and 4, respectively. These particle morphologies do not represent discrete intermediates formed at certain steps during the reaction defined by a specific reaction time, but evolve out of each other. Consequently different intermediates can exist next to each other at a given time during reaction. The intermediates reported below are the respective major fraction at a particular time. The SEM images of the respective intermediates are shown in Figure 1. Figure 1 a depicts the first intermediate (Intermediate 1) that has been isolated after about 4 h. An overview and detailed SEM pictures of single Intermediate 1 particles are provided in Figure S1 in the Supporting Information. It is composed of spherical Sb_xTe_y nanoparticles with an average diameter of 140 ± 30 nm and an EDX analysis reveals an average Sb/Te ratio of 0.47. These particles are amorphous according to powder X-ray diffraction (Figure S2a) and are thus considered to be a non-stoichiometric alloy. In addition we recorded TEM and SAED data with an aperture that corresponds to the diameter of Intermediate 1 (cf. Figure S2d and e). The diffuse reflection underlines the amorphous state of Intermediate 1, which is in accordance to the X-ray diffraction data. These particles evolve into Intermediate 2, a structure resembling a "fried egg" shape by the formation of a corona-like layer around a spherical core (Figure 1). Overview images as well as detailed SEM pictures of single Intermediate 2 particles are provided in Figure S3. AFM measurements reveal that this corona-like structure is composed of one or two individual layers having a thickness of approximately 6 nm (first layer) and approximately 7.5 nm (second layer; Figure S4). EDX analysis of the structure shows the presence of Sb and Te in the core as well as the layer region. However, the structure is too thin to allow quantification of both elements by EDX (Figure S5). Intermediate 3 evolves from the irregularly shaped "fried egg" structure. It has a hexagonal shape (Figure 1 c and Figure S8),

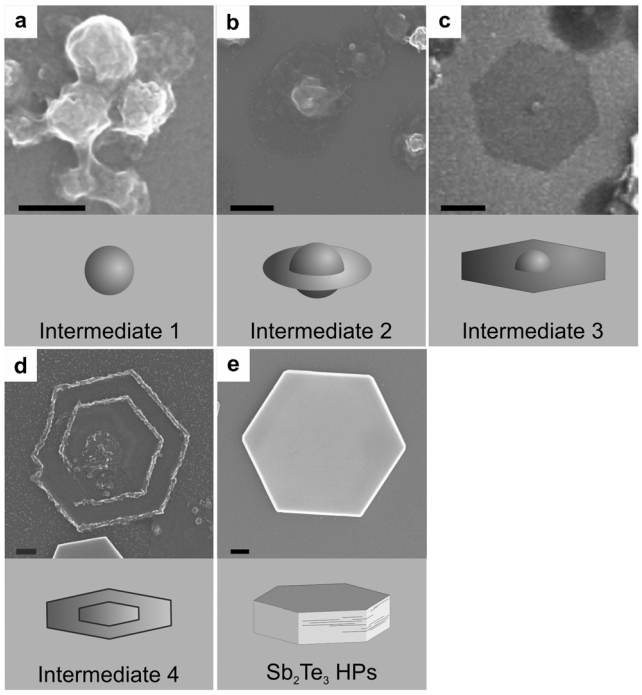

Figure 1. Series of SEM images of intermediates identified during the solvothermal synthesis of Sb_2Te_3 and corresponding simplified models that illustrate the respective morphologies. a) Intermediate 1, amorphous spherical Sb_xTe_y particles, b) Intermediate 2, "fried egg" like structure, c) Intermediate 3, evolution of a hexagonal shape, d) Intermediate 4, hexagonally shaped layers with convex rim e) final Sb_2Te_3 hexagonal platelets. scale bar: 200 nm.

and AFM measurements again reflect a layer thickness of approximately 6.5 nm (Figure S9). From the shape and the homogeneous layer thickness, a crystalline structure may tentatively be assumed.

In Intermediate 4 the hexagonal shape is retained and additionally a convex outer rim is formed (Figure 1 d and Figure S11). The layers between core and rim appear to be more uniform and dense compared to Intermediate 3 as judged from the SEM image (Figure S11c). The layer thickness remains at approximately 6 nm in this stage (Figure S12). EDX analysis of this intermediate shows that Te and Sb can be found in the core, in the rim, as well as in the layer. Owing to the low thickness, quantitative EDX results cannot be obtained (Figure S13). Eventually further crystal growth and ripening led to the final Sb_2Te_3 hexagonal platelets (Figure 1 e).

The intermediate structures found in this series of measurements reflect a formation mechanism, which starts with the formation of amorphous, spherical Sb–Te alloy nanoparticles changing first into an irregular and then into a regular, hexagonally shaped layered structure, which has an invariant layer thicknesses of approximately 6 nm. This formation process ends up with the appearance of regularly shaped hexagonal platelets. However, it should be noted that only Intermediate 1, that is, the SbTe alloy nanoparticles, and the final product, that is, the hexagonal platelets, could be analyzed in pure form for crystallinity by means of X-ray diffraction. Intermediates 2–4 could not be obtained as pure, but as majority compounds of a mixture. Thus, the assumption that the layer structures are crystalline is simply deduced from the invariant layer height and the hexagonal shape. To verify this assumption, we performed STEM and ND measurements on these intermediates.

ND with 2 nm resolution has been performed.[15] Together with the precise positioning of the electron beam and the low energy input, area-resolved crystallinity mappings without affecting the sample structure can be obtained. For the measurements, TEM samples were prepared by drop drying a highly diluted dispersion of the isolated intermediates on a carbon-coated copper grid.

Figure 2 a–c depicts the STEM images of the different intermediate structures identified during the growth process and includes marks showing the positions of recorded ND patterns. Figure 2 a shows Intermediate 2, Figure 2 b Intermediate 3, and Figure 2 c corresponds to the Intermediate 4 shown in Figure 1 d with the more compact layer between the core and convex rim.

Dark spots on the first-formed layer of the "fried egg" structures in Figure 2 a and b suggests that this layer has a more porous structure. On the right hand side of the STEM images of the intermediates, two diffraction patterns, recorded at the locations marked in the STEM images with X_1 and X_2, are shown. The ND pattern determined in the core region shows clear reflections, whereas the ND pattern measured at the layer only shows diffuse scattering (Figure 2 a X_1 and X_2 and Figure S6). A more detailed ND analysis of another core region reveals that the crystalline region itself can also have a smaller diameter than the core region itself (Figure S7). Figure 2 b shows similar results, reflecting a partially crystalline core surrounded by an amorphous corona. Additional diffraction patterns are shown in Figure S10. However, the "fried egg" structure approaches a hexagonal shape and has a much more uniform contrast compared to that in Figure 2 a, indicating a uniform thickness, which is consistent with the AFM measurements suggesting a layer thickness of about 6 nm (Figure S9).

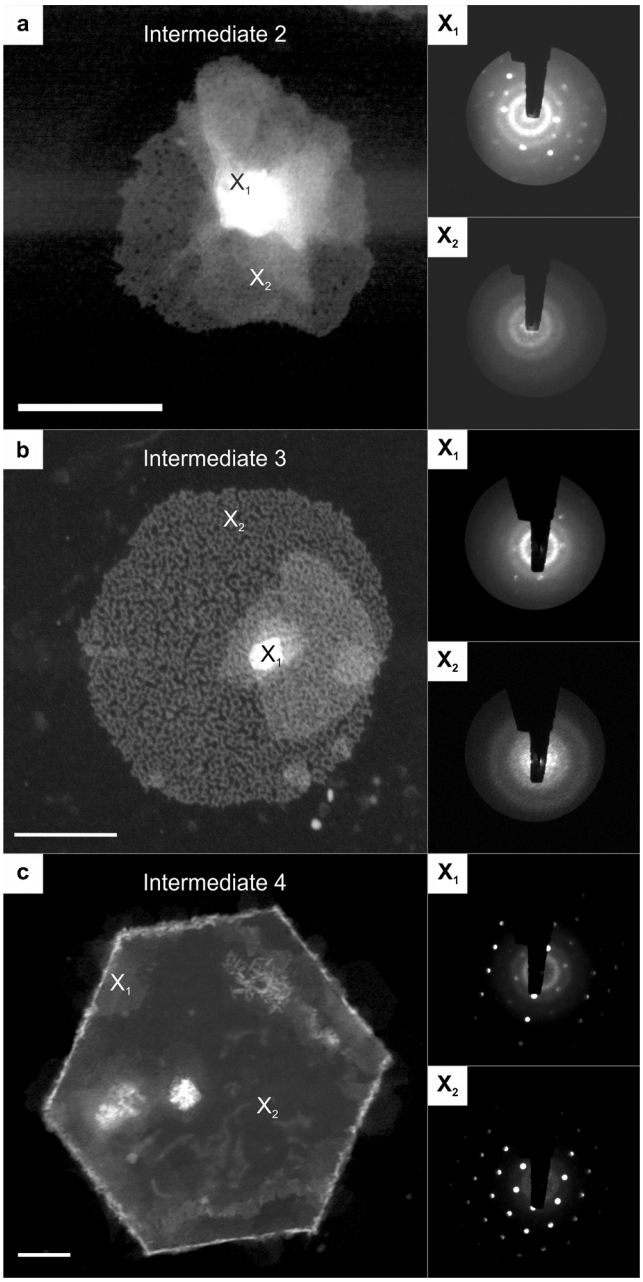

Figure 2. STEM Images and corresponding diffraction patterns from ND measurements. a) "Fried egg" like intermediate structure (Intermediate 2) with the corresponding diffraction images X_1 and X_2 showing the crystalline nature of the core and amorphous nature of the initially formed layer. b) "Fried egg" structure with hexagonal shape (Intermediate 3) and diffraction patterns X_1 of the crystalline core and X_2 the amorphous layer. c) Intermediate 4 with the first crystalline Sb_2Te_3 layer and the corresponding diffraction patterns X_1 and X_2 depicting the same pattern only differing in the reflection intensities. Scale bar: 200 nm.

Even the growth of a second layer, uniform in thickness, can be observed through the resulting higher contrast. This is an intriguing finding, as the results suggest that the hexagonal shape and the uniform, clearly discriminable layer represent a crystalline structure, whereas the ND analyses reveal an at least partly crystalline structure for only the core region, but not in the corona region.

Finally, Figure 2c shows a hexagonal structure with a more-compact layer between core and convex rim. This layer is entirely crystalline as the diffraction patterns show. Moreover, this layer shows the same crystal orientation at every measured spot; only differences in the diffraction intensity arising from variations of the incident angle of the electron beam are observable (Figure S14). The diffraction pattern could be assigned to the diffraction pattern of Sb_2Te_3 by an overlay with a theoretical pattern calculated by the program JEMS (Figure S15). The basal plane of Intermediate 4 is oriented parallel to the carbon layer of the copper grid.

To demonstrate that the solvothermally synthesized Sb_2Te_3 hexagonal platelets exhibit electrical phase-change switching properties, we performed first electrical switching experiments on individual crystals. Since standard lithographic methods are not suited to electrically address individual crystals selectively and non-destructively, we applied an in situ nanomanipulator setup integrated in a SEM (Figure 3a).[16] This setup allows the electrical properties of individual crystals contacted by two metallic tips to be measured during visual inspection of the SEM (Figure 3c).

As a first step the electrical resistance was recorded and revealed values around 5 kΩ for the tip–hexagonal platelets–tip configuration, the values slightly varying with the position of the tips. This variation is attributed to the surface roughness of the hexagonal platelets as well as of the measuring tip, which lead to variation in the contact area. To elucidate the appropriate pulse width needed to locally amorphize the electrically addressed hexagonal platelets, we applied a series of pulses of 0.75 volt height and increasing pulse width starting with 25 ns pulses. After each pulse the resistance was measured by a $I(U)$ sweep with a range from −0.01 to 0.01 V and back. The resulting plot of pulse width against resistance (Figure S16) shows for pulses between 25 and 135 ns a resistance between 2 to 10 kΩ for the tip–hexagonal platelets–tip configuration. Application of a 145 ns pulse leads to drastically increased resistance of 800 MΩ implying that the material around the voltage-imposing right tip has locally been amorphized. This represents the RESET process. To show the phase-change switching characteristic we applied a switching sweep starting at 0 V going to 5 V and back with a compliance current (CC) of 1 μA (Figure 3b). We observed the typical unipolar switching characteristic for phase-change materials being switched from the HRS state to the LRS state with a SET voltage of 1.1 V. In a series of 16 measurements composed of 13 measurements for resistance determination followed by three switching sweeps we observed a slight thermal drift of the measurement tips. However, the switching process itself was unaffected by this. In our experiments only three switching cycles could be measured after which the system is remains in the LRS. This might be explained by our

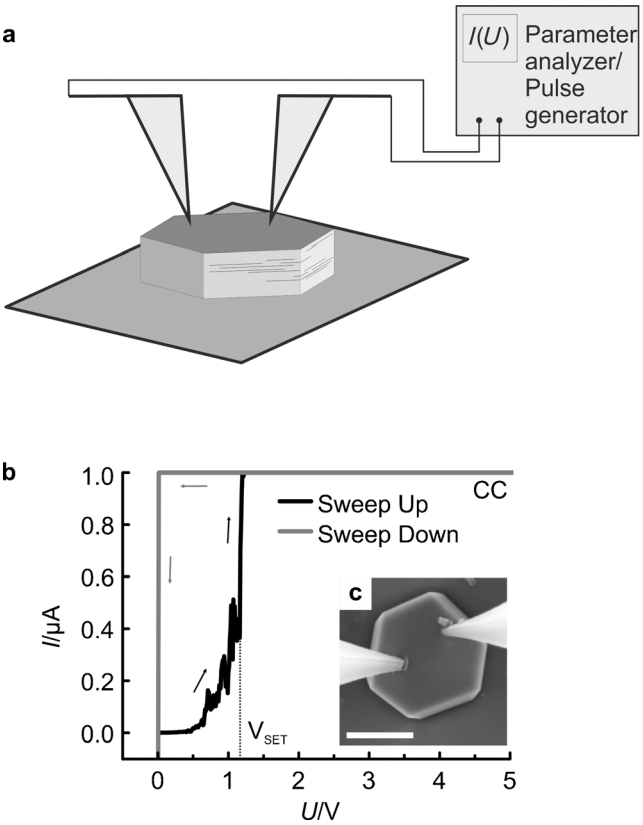

Figure 3. a) Measuring setup in the SEM. b) Switching sweep measured for an in situ contacted Sb_2Te_3 hexagonal platelet in the SEM. c) Positions of the measuring tips during measurement the switching events. Scale bar: 1 μm.

measurements conditions, as the switching experiments are carried out in a SEM under vacuum. Other phase-change devices, which are equipped with a capping layer, can be switched up 10^{11} times.[17] In our systems, tellurium which is the component with the highest vapor pressure can evaporate during the RESET switching. This leads to phase segregation and eventually to the loss of the phase-change properties.[18]

In summary, we solvothermally synthesized Sb_2Te_3 hexagonal platelets and studied the evolution of distinguishable intermediates along the reaction path of the final product. These intermediates show a peculiar amorphous to crystalline transition in the course of their evolution. First amorphous NPs are formed with a Sb/Te ratio of 0.47, denoted as Intermediate 1. These evolve to Intermediate 2, which resembles a "fried egg" structure with a corona-like layer revealing a uniform thickness. ND analysis shows that this entire intermediate is amorphous except for a small crystalline region in the core particle. Intermediate 3 is formed by a shape evolution of the outer layer from an irregular to a hexagonal outer shape, whereas the layer is still amorphous. We consider this as an intriguing formation mechanism, as the hexagonal structures are composed of an apparently amorphous material. Finally the synthesis yields single-crystalline Sb_2Te_3 hexagonal platelets. In addition we could demonstrate for the first time resistive switching on individual hexagonal platelets showing the typical characteristics of a phase-change material.

Our results give an insight into the formation mechanism of the technically relevant material Sb_2Te_3 in solvothermal synthesis. This information may potentially help to control the size and shape of individual crystals. The evidence of resistive phase-change switching makes the chemically synthesized Sb_2Te_3 suited for application in data-storage devices.

Keywords: amorphous intermediates · in situ measurements · nanodiffraction · phase change · solvothermal synthesis

How to cite: *Angew. Chem. Int. Ed.* **2015**, *54*, 6632–6636
Angew. Chem. **2015**, *127*, 6732–6736

[1] M. Wuttig, *Phys. Status Solidi B* **2012**, *249*, 1843–1850.
[2] a) R. Metha, Y. Zhang, C. Karthik, B. Singh, R. Siegel, T. Borca-Tasciuc, G. Ramanath, *Nat. Mater.* **2012**, *11*, 233–240; b) S. Zastrow, J. Gooth, T. Boehnert, S. Heienrich, W. Toellner, S. Himann, S. Nielsch, *Semicond. Sci. Technol.* **2013**, *28*, 035010.
[3] a) H. Zhang, C. Liu, X. Qi, X. Dai, Z. Fang, S. Zhang, *Nat. Phys.* **2009**, *6*, 438–442; b) L. Plucinski, A. Herdt, S. Fahrendorf, G. Bihlmayer, G. Mussler, S. Döring, J. Kampmeier, F. Matthes, D. Bürgler, D. Grützmacher, S. Blügel, C. Schneider, *J. Appl. Phys.* **2013**, *113*, 053706.
[4] a) D. Lencer, M. Salinga, B. Grabowski, T. Hickel, J. Neugebauer, M. Wuttig, *Nat. Mater.* **2008**, *7*, 972–977; b) S. Raoux, W. Wełnic, D. Ielmin, *Chem. Rev.* **2010**, *110*, 240–267.
[5] R. Wyckoff, *Crystal Structures 2*, Wiley, New York, **1964**.
[6] a) Z. Hurych, R. Benbow, *Phys. Rev. B* **1977**, *16*, 3707–3712; b) V. Wagner, G. Dolling, B. Powell, G. Landwehr, *Phys. Status Solidi B* **1978**, *85*, 311–317.
[7] a) M. Wuttig, N. Yamada, *Nat. Mater.* **2007**, *6*, 824–832.
[8] a) J. Oh, S. Ryu, R. Choi, S. Choi, C. Hwang, H. Kim, S. Hwang, Y. Kim, H. Park, H. Chang, S. Hong, *J. Korean Phys. Soc.* **2006**, *49*, 1173–1179; b) S. Raoux, *Annu. Rev. Mater. Res.* **2009**, *39*, 25–48; c) C. Peng, L. Wu, Z. Song, F. Rao, M. Zhu, X. Li, B. Liu, L. Cheng, S. Feng, P. Yang, J. Chu, *Appl. Surf. Sci.* **2011**, *257*, 10667–10670; d) B. Lee, K. Darmawikarta, S. Raoux, Y. Shih, Y. Zhu, S. Bishop, J. Anderson, *Appl. Phys. Lett.* **2014**, *104*, 071907.
[9] a) S. Barnett, I. Fergusson, *Handbook in Thin Film Process Technology* (Eds.: S. Shah, D. Glockner), Institute of Physics Publishing, Bristol, **1995**, A2.0:1–A2.0.35; b) I. Shah, *Handbook in Thin Film Process Technology* (Eds.: S. Shah, D. Glockner), Institute of Physics Publishing, Bristol, **1995**, A3.0:1–A3.0.18; c) L. Vescan, *Handbook in Thin Film Process Technology* (Eds.: S. Shah, D. Glockner), Institute of Physics Publishing, Bristol, **1995**, B2.0:1-B2.0.12.
[10] a) Y. Zhao, C. Burda, *ACS Appl. Mater. Interfaces* **2009**, *1*, 1259–1263; b) H. Kim, K. Lee, S. Kim, M. Han, *Bull. Korean Chem. Soc.* **2010**, *31*, 1123–1127.
[11] a) S. Garje, D. Eisler, J. Ritch, M. Afzaal, P. O'Brien, T. Chivers, *J. Am. Chem. Soc.* **2006**, *128*, 3120–3121; b) S. Schulz, S. Heimann, J. Friedrich, M. Engenhorst, G. Schierning, W. Assenmacher, *Chem. Mater.* **2012**, *24*, 2228–2234.
[12] a) W. Wang, B. Poudel, J. Yang, D. Wang, Z. Ren, *J. Am. Chem. Soc.* **2005**, *127*, 13792–13793; b) W. Shi, L. Zhou, S. Song, J. Yang, H. Zhang, *Adv. Mater.* **2008**, *20*, 1892–1897; c) G. Dong, Y. Zhu, L. Chen, *J. Mater. Chem.* **2010**, *20*, 1976; d) G. Dong, Y. Zhu, L. Chen, *CrystEngComm* **2011**, *13*, 6811–6816; e) R. Jin, G. Chen, C. Yan, D. Chen, H. Xu, J. Pei, *CrystEngComm* **2012**, *14*, 8547–8553; f) R. Jin, G. Chen, J. Pei, H. Xu, Z. Lv, *RSC Adv.* **2012**, *2*, 1450–1456; g) S. Sun, J. Peng, R. Jin, S. Song, P. Zhu, Y. Xing, *J. Alloys Compd.* **2013**, *558*, 6–10; h) J. Yang, P. Zuo, P. S. Zhang, B. Jin, Y. Tian, J. Yang, *J. Alloys Compd.* **2013**, *565*, 73–78.
[13] a) Y. Min, G. Moon, C. Kim, J. Lee, H. Yang, A. Soon, U. Jeong, *J. Mater. Chem. C* **2014**, *2*, 6222; b) M. Ferhat, J. Tedanac, J. Nagao, *J. Cryst. Growth* **2000**, *218*, 250–258.
[14] G. Zhang, W. Wang, X. Lu, X. Li, *Cryst. Growth Des.* **2009**, *9*, 145–150.
[15] J. Zuo, J. Tao in *Scanning Transmission Electron Microscopy—Imaging and Analysis* (Eds.: S. Pennycook, P. Nellist), Springer, Heidelberg, **2011**, pp. 393–429.
[16] M. Noyong, K. Blech, A. Rosenberger, V. Klocke, U. Simon, *Meas. Sci. Technol.* **2007**, *18*, N84–N89.
[17] S. Raoux, F. Xiong, M. Wuttig, E. Pop, *MRS Bull.* **2014**, *39*, 703–710.
[18] a) L. Krusin-Elbaum, C. Cabral, K. Chen, M. Copel, D. Abraham, K. Reuter, S. Rossnagel, J. Bruley, *Appl. Phys. Lett.* **2007**, *90*, 141902; b) L. Goncalves, P. Alpuim, A. Rolo, J. Correia, *Thin Solid Films* **2011**, *519*, 4152–4157.

Received: January 13, 2015
Revised: February 16, 2015
Published online: April 13, 2015

